Longitudinal and transverse structure functions in decaying nearly homogeneous and isotropic turbulence*

Imtiaz Ahmad[a)b)], Lu Zhi-Ming(卢志明)[a)†], and Liu Yu-Lu(刘宇陆)[a)]

[a)] *Shanghai Key Laboratory of Mechanics in Energy Engineering, Shanghai Institute of Applied Mathematics and Mechanics, Shanghai University, Shanghai* 200072, *China*

[b)] *Department of Mathematics, University of Azad Jammu and Kashmir, Muzaffarabad* 13100, *Pakistan*

(Received 19 March 2013; revised manuscript received 23 June 2013; published 12 November 2013)

Streamwise evolution of longitudinal and transverse velocity structure functions in a decaying homogeneous and nearly isotropic turbulence is reported for Reynolds numbers Re_λ up to 720. First, two theoretical relations between longitudinal and transverse structure functions are examined in the light of recently derived relations and the results show that the low-order transverse structure functions can be well approximated by longitudinal ones within the sub-inertial range. Reconstruction of fourth-order transverse structure functions with a recently proposed relation by Grauer *et al*. is comparatively less valid than the relation already proposed by Antonia *et al*. Secondly, extended self-similarity methods are used to measure the scaling exponents up to order eight and the streamwise evolution of scaling exponents is explored. The scaling exponents of longitudinal structure functions are, at first location, close to Zybin's model, and at the fourth location, close to She–Leveque model. No obvious trend is found for the streamwise evolution of longitudinal scaling exponents, whereas, on the contrary, transverse scaling exponents become slightly smaller with the development of a steamwise direction. Finally, the stremwise variation of the order-dependent isotropy ratio indicates the turbulence at the last location is closer to isotropic than the other three locations.

Keywords: fully developed turbulence, longitudinal and transverse structure functions, scaling exponents, intermittency

PACS: 47.10.ad, 47.27.Jv **DOI:** 10.1088/1674-1056/23/1/014701

1. Introduction

Theory of turbulence and development of calculation methods for high-Reynolds number flow is a challenging research topic.[1] Structure functions are widely studied in turbulence because they contain basic information about small-scale motion and capture local and non-local effects inherent to turbulent flows.[1,2] Two types of Eulerian structure functions are frequently being used to study the statistical properties of turbulence, i.e., longitudinal structure functions, $S_{\rm L}^p(r) = \langle (u(x+r)-u(x))^p \rangle = \langle \Delta u_r{}^p \rangle$ and transverse structure functions $S_{\rm T}^p(r) = \langle (v(x+r)-v(x))^p \rangle = \langle \Delta v_r{}^p \rangle$, where $\langle \cdot \rangle$ denotes the ensemble average, p is the order of structure functions, u, v are the velocity components parallel and perpendicular to the mean flow respectively and r is the separate distance. The issue of a scaling behavior of structure functions was addressed for the first time inKolmogorov's theory in 1941 (hereafter referred to as the K41 theory), when he proposed the concept of self-similarity of an inertial range in turbulence. According to K41 theory, for locally homogenous and isotropic turbulence at high Reynolds numbers, $p^{\rm th}$-order structure functions scale as r^{ζ^p} and scaling exponent ζ^p increases linearly with the order of structure functions. Explanation of departure of scaling exponents from the K41 theory or self-similarity, usually referred to as anomalous scaling, is one of the great problems in the study of turbulence. Kolmogorov presented a refined similarity hypothesis to account for the intermittency, a violation of self-similarity, in 1962 (hereafter referred to as K62 theory).[3,4] According to K41 and K62 theories, the cascade process is universal and both $\zeta_{\rm L}^p = \zeta_{\rm T}^p$, but proved only for $n = 2$ and 3. The theory, in general, is supported by the argument of Biferale and Procaccia that if the longitudinal and the transverse structure functions had different scaling exponents, then there will be no scaling in all the other directions.[5] However, only a few studies partially supported the identical nature of $\zeta_{\rm L}^p$ and $\zeta_{\rm T}^p$.[6–8] Regardless of theoretical arguments, experimental studies and direct numerical simulations (DNS) concluded that higher-order $\zeta_{\rm T}^p$ is smaller than $\zeta_{\rm L}^p$ of the same order and hence the intermittency corrections of transverse velocity fluctuations $\delta\zeta_{\rm T}^p = \zeta_{\rm T}^p - p/3$ are stronger than that of longitudinal ones $\delta\zeta_{\rm L}^p = \zeta_{\rm L}^p - p/3$ when $p > 3$.[9–14] It is argued that the difference is due to deviations from the ideal conditions, such as local homogeneity, a lack of inertial range isotropy and different levels of intermittency effects on longitudinal and transverse structure functions.[5,15,16] In such studies, it is believed that for highly isotropic flows when the Reynolds numbers become large enough, the difference will be negligible.[6,15,17]

For different kinds of turbulence, there are many studies

*Project supported by the National Natural Science Foundation of China (Grant Nos. 11272196, 11002085, and 11032007) and the Key Project of Education Commission of Shanghai Municipal, China (Grant No. 11ZZ87).

†Corresponding author. E-mail: zmlu@shu.edu.cn

© 2014 Chinese Physical Society and IOP Publishing Ltd

available, some of which investigate the dependence of scaling exponents on the vertical distance from the wall and others gave a comparison of the ζ_L^p and ζ_T^p.[6,11,12,18–21], However, the streamwise evolution and comparison of ζ_L^p and ζ_T^p in a decaying turbulent flow is rarely studied. The primary aim of this work is to investigate the streamwise evolution of ζ_L^p and ζ_T^p in channel flow turbulence and the difference between ζ_L^p and ζ_T^p at various locations. Our secondary aim deals with the statistical link between longitudinal and transverse structure functions. Transverse structure functions could be reconstructed via equivalent order of longitudinal structure functions and their derivatives.[22–24] We try to reconstruct low-order transverse structure functions from the the same order of longitudinal structure functions and their derivatives using some derived formulas. We focus on a recently published work of Grauer *et al.* who reconstructed transverse structure functions of the order up to ten.[24]

The rest of the paper is organized as follows. In Section 2, we present some key features of experimental dataset being used in this study. In Section 3, utilizing the experimental dataset, we discuss some relations between longitudinal and transverse structure functions where our focus is the link between transverse and longitudinal structure functions. In Section 4, we measure longitudinal and transverse structure functions at four locations and discuss streamwise evolution of their scaling exponents in the light of classical intermittency models and some relevant experimental and DNS results. Finally, concluding remarks are drawn in Section 5.

2. Experimental data

The database is obtained experimentally in decaying nearly homogeneous isotropic turbulence. An active-grid technique at the entrance of the wind tunnel is used to achieve high Reynolds numbers. The data is measured using HWA at four downstream locations, i.e., at $x/M = 20, 30, 40$ and 48 where M is the mesh size. The sampling frequency, f_s, is 40 kHz. The sampling time is 30 s for each measurement and 30 measurements are carried out for each location. Therefore, the total number of data points at each location is $30 \times 1.2 \times 10^6$. The details about the experimental set and measuring techniques are available in Ref. [25]. The data, originally measured in the temporal domain, is transformed into the spatial domain by invoking Taylor's hypothesis. The mean velocities $\langle u \rangle$ at these four locations range from 12.0 m·s^{-1}–10.8 m·s^{-1}.

Taylor's micro-scale based Reynolds numbers Re_λ and turbulent intensities also decrease continuously and slowly from the first to the fourth measurement location. The range of Re_λ is 720–620 with turbulent intensities 15.4%–10.0%. On the other hand, anisotropy ratios increase from 1.13 at the first location to 1.16 at the last location. Some other parameters of the database are given in Table 1. Figure 1 shows the energy spectra of longitudinal (blue solid lines) and transverse (magenta

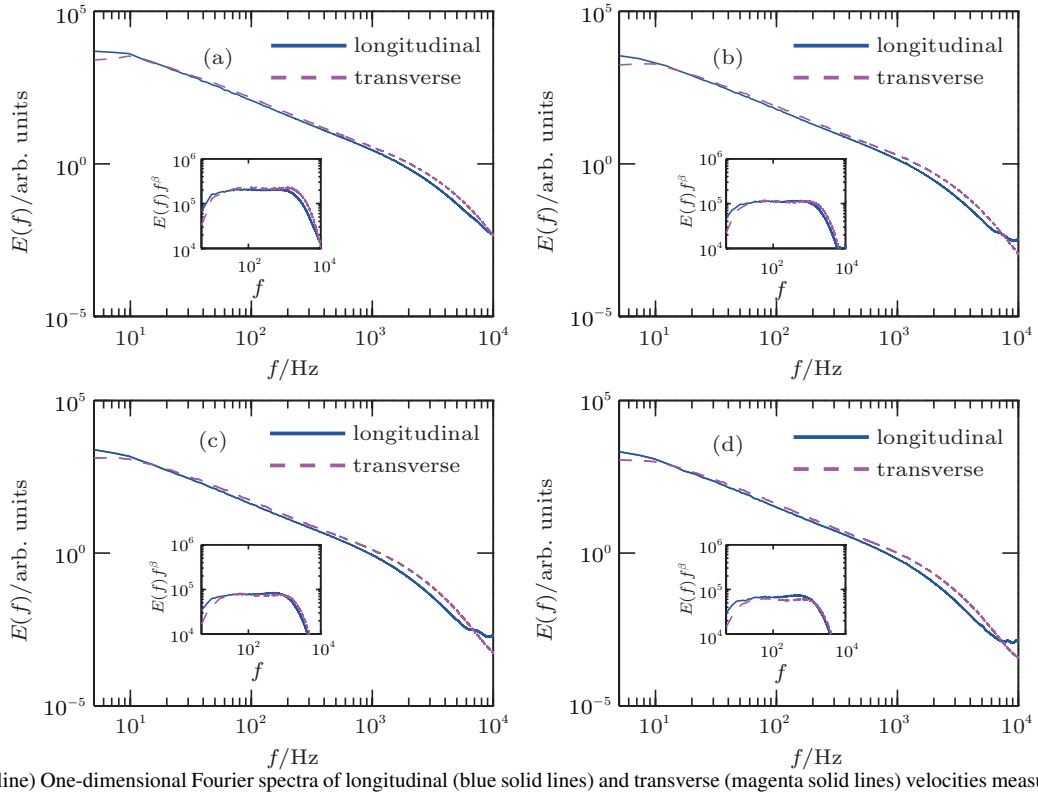


Fig. 1. (color online) One-dimensional Fourier spectra of longitudinal (blue solid lines) and transverse (magenta solid lines) velocities measured at $x/M = 20$ (a), 30 (b), 40 (c) and 48 (d), where M is the mesh size shown in (a)–(d). The inertial-ranges lie in the intervals 20 Hz $< f <$ 1000 Hz approximately, the corresponding time separation ranges are 0.001 s $< \tau <$ 0.05 s where the power law with slopes $\simeq -5/3$ can be observed. The insets show compensated spectra $E(f)f^\beta$, measured at the above mentioned four locations with the same line styles and color schemes.

Table 1. Some basic parameters of the experimental database measured at four streamwise locations.

	$x/M=20$	$x/M=30$	$x/M=40$	$x/M=48$
$\langle u_1\rangle$/(m/s)	12.0	11.2	11.0	10.8
u_{1rms}/(m/s)	1.85	1.43	1.19	1.08
$u_{1rms}/\langle u_1\rangle$/(%)	15.4	12.8	10.8	10.0
$I=\frac{u_{1rms}}{u_{2rms}}$	1.13	1.14	1.14	1.16
η/mm	0.11	0.14	0.16	0.18
λ/mm	5.84	7.13	8.25	8.78
$Re_\lambda=\frac{u_{1rms}\lambda}{\nu}$	716	676	650	626

dashed lines) velocities measured at four locations where the insets show the respective compensated spectra $E(f)f^\beta$ measured at the four locations. These spectra indicate that the inertial-ranges, at four measurement locations for both velocities, lie approximately 20 Hz $< f <$ 1000 Hz. Thus, both velocities exhibit power-law behaviors at all four locations for a range of nearly two decades. At all four locations, values of scaling exponents β, for transverse velocities, is $\simeq -1.59$ whereas for longitudinal velocities, it increases slowly from -1.62 at the first location to -1.66 at the last location, which is closer to the theoretical value $-5/3$. The scaling exponents are consistent with the observation of Saddoughi and Veeravalli[26] who mentioned that the spectrum of transverse velocity may be slightly less steep than the spectrum of the longitudinal velocity. This observation is confirmed by Sreenivasan and Zhou *et al.* who showed, with different flows at different Re_λ, that the transverse velocity spectrum attains $-5/3$ slope only at very high Reynolds numbers.[27,28] Another notable thing is that scaling ranges of longitudinal and transverse spectra is nearly the same, which is consistent to the findings of Shen and Warhaft.[6]

3. Relation between longitudinal and transverse structure functions

A famous exact relation between second-order longitudinal and transverse structure functions for incompressible isotropic turbulence derived by Kármán and Howarth in 1938 is

$$S_{\rm T}^2(r)=S_{\rm L}^2(r)+\frac{r}{2}\frac{\partial}{\partial r}S_{\rm L}^2(r), \tag{1}$$

which contains no contribution from the pressure and is commonly used to measure the anisotropy of turbulent flows. Differentiation of turbulence data increases noises; to restrict noises, before differentiation with respect to r, we use high-order polynomial fitting to these low-order structure functions. In Fig. 2, we reconstruct a second-order transverse structure function from the longitudinal one according to Eq. (1) and plot it together with the measured second-order longitudinal and transverse structure functions for comparison. In the inset, we plot the percentage of error of Eq. (1) at all four locations. The reconstruction works well around 10% of accuracy at the first location and within 30% of accuracy at the remaining three locations, in the inertial range. The reconstructed and actual (measured) second-order transverse structure functions share the same inertial range and scaling exponents.

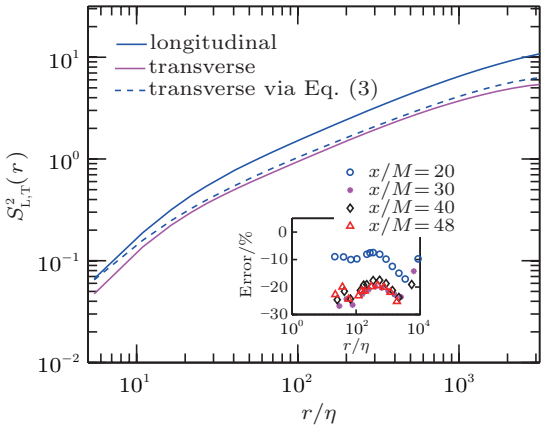


Fig. 2. (color online) Plots of second-order longitudinal structure functions (blue solid line), transverse structure functions (magenta solid line) and second-order transverse structure functions reconstructed by Eq. (1) (blue dashed line). The blue solid line is shifted up for a better representation. The inertial range is enclosed within the vertical dashed lines. The inset shows the percentage of error, ((LHS–RHS)/LHS)×100, for Eq. (1) at all four locations.

A large amount of work has been devoted to address the relations between higher-order longitudinal and transverse structure functions.[16,22–24,30,31] A recent effort was made by Grauer *et al.* who extended the relations for higher-order structure functions and, by ignoring the contributions from the pressure and large-scale forcing, they expressed transverse structure functions, up to order ten, in terms of longitudinal structure functions.[24] For example, the fourth-order transverse structure function is reconstructed with the longitudinal one as

$$S_{\rm T}^4(r)=S_{\rm L}^4(r)+r\frac{7}{8}\frac{\partial}{\partial r}S_{\rm L}^4(r)+r^2\frac{1}{8}\frac{\partial^2}{\partial r^2}S_{\rm L}^4(r). \tag{2}$$

The above formula is different from Antonia *et al.*'s model, which has been examined by themselves in a plane jet flow at a similar Reynolds number to that of this article.[32] To find the difference, we include Antonia *et al.*'s formula as below

$$S_{\rm T}^4(r)=S_{\rm L}^4(r)+r\frac{9}{16}\frac{\partial}{\partial r}S_{\rm L}^4(r)+r^2\frac{1}{16}\frac{\partial^2}{\partial r^2}S_{\rm L}^4(r). \tag{3}$$

In Fig. 3, we reconstruct fourth-order transverse structure functions from the longitudinal one according to Eqs. (2) and (3), and plot them together with the measured fourth-order longitudinal and transverse structure functions for comparison. It is clearly seen that Eq. (3) gives a much better approximation, and from points of inertial range and scaling exponents, both equations (2) and (3) give the same results as the measured one. In the insets, the relative errors of Eqs. (2) and (5), measured at all locations, are shown on the top-left and bottom-right respectively. It is seen again, the relative errors

of Eq. (3) are much smaller than those of Eq. (2); it is interesting to notice that these errors, with both formulas, at the first locations are smaller than those measured at other locations but increase with downstream locations without any particular trends. Overall, a better reconstruction of fourth-order transverse structure functions is achieved with the formula proposed by Antonia *et al.* Figures 2 and 3 show that the second- and fourth-order transverse structure functions can be reconstructed, in the inertial range, by corresponding order of longitudinal structure functions and their derivatives with the dataset being used. The reconstructed transverse structure functions share the same inertial range where the power-law behavior is observed, although the scaling exponents are slightly different.

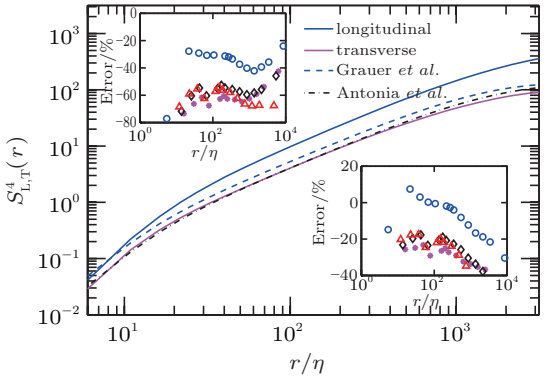


Fig. 3. (color online) Plots of fourth-order longitudinal (blue solid line) and transverse (magenta solid line) structure functions whereas the blue dashed line and black dot-dashed line represent fourth-order transverse structure functions reconstructed by Eqs. (2) and (3), respectively. The blue solid line is shifted up for better representation. The top-left and bottom-right insets show percentage error, ((LHS–RHS)/LHS)×100, for Eqs. (2) and (3) at all four locations respectively. The legends for both insets are the same as those of inset in Fig. 2.

To see the difference between the formulas proposed by Grauer *et al.* and Antonia *et al.* more clearly, we define a fourth-order isotropy ratio $I^4 = \langle S^4_{\rm L}/S^4_{\rm T}\rangle$ where an average is taken within the inertial range. Taking Kolmogorov's second similarity hypothesis, we have the inertial range $S^4_{\rm L} = Cr^{4/3}$ and $S^4_{\rm T} = C'r^{4/3}$, where C and C' are the universal constants. From Eqs. (2) and (3), it is easy to obtain in the inertial range, $I^4 = 9/20$ and $9/16$ respectively. We plot measured $S^4_{\rm L}/S^4_{\rm T}$ at all four locations in Fig. 4. It is shown that, in the inertial range, the ratios, at all four locations, are closer to the ratios calculated according to the formula of Antonia *et al.* (dashed magenta line) and far from the ratio calculated from the Grauer *et al.* formula (solid blue line). This is a clear indication that the formula derived by Antonia *et al.* is a better approximation of fourth-order transverse structure function than that derived by Grauer *et al.*

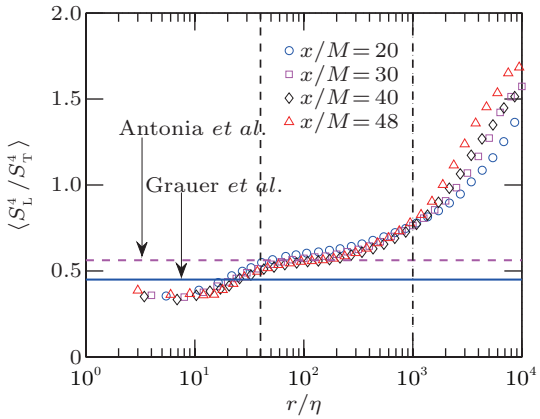


Fig. 4. (color online) Isotropy ratios $S^4_{\rm L}/S^4_{\rm T}$ of fourth-order longitudinal to transverse structure functions as a function of separation scales, measured from experimental data at four downstream locations, i.e., $x/M = 20, 30, 40$ and 48. Inertial range is enclosed within vertical dashed lines whereas two horizontal lines represent ratios obtained by applying Kolmogorov theory on formulas derived by Grauer *et al.* (blue solid line) and Antonia *et al.* (magenta dashed line).

4. Streamwise evolution of scaling exponents

To estimate the maximum degree of the order of structure functions that can be measured accurately, integral kernels, i.e., $P(\Delta u_r)\Delta u_r{}^p$ are evaluated where $P(\Delta u_r)$ is the probability density function of the longitudinal velocity difference over the separation distance r for several typical separation scales at all four locations; it is concluded that the highest value of p for which an acceptable signale-to-noise ratio can be obtained is eight. Now, we investigate the longitudinal and transverse structure functions at four streamwise locations. Figure 5 shows structure functions $S^p_{\rm L}(r)$ and $S^p_{\rm T}(r)$ as a function of r/η measured at four locations, i.e., $x/M = 20, 30, 40$ and 48 in Figs. 5(a), 5(b), 5(c) and 5(d) respectively. It is observed that, first, the values of both longitudinal and transverse structure functions decrease with the increase of the streamwise distance from the grid; second, the slopes of the longitudinal structure functions are larger than those of transverse ones of the same order; third, a very good power-law behavior is seen for lower-order structure functions in the inertial range and it is comparatively worse for high-order ones as expected. So we resort to the extended self-similarity method (ESS) introduced by Benzi *et al.*[34,35] to extract the scaling exponents.

In Fig. 6, we plot scaling exponents of longitudinal and transverse structure functions using ESS measured at four streamwise locations, i.e., $x/M = 20, 30, 40$ and 48 along with the K41 model. The She and Leveque (S–L) model is among one of the most accepted models proposed to describe the anomalous scaling of ζ^p.[33] The Zybin *et al.* model is one of most recent models, which is based on a particular solution of Navier–Stokes equations and claims to have a better solid foundation.[31] Here, in Fig. 6, S–L and Zybin *et al.* models are not plotted for sake of clarity but we will compare our measurements with these models in Table 2. It is evidently seen from Fig. 6 that both $\zeta^p_{\rm L}$ and $\zeta^p_{\rm T}$ show a departure from

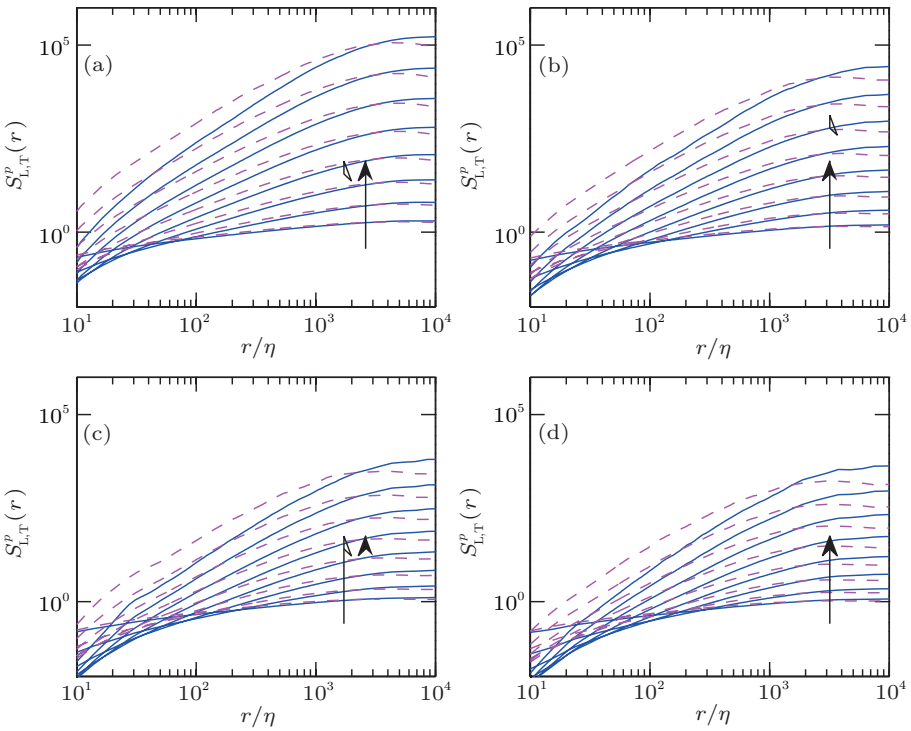


Fig. 5. (color online) Longitudinal and transverse velocity structure functions $S^p_{\mathrm{L,T}}(r)$ as functions of r/η for $p = 1,2,...,8$ measured at four locations, i.e., $x/M = 20,30,40$ and 48 are shown in panels (a)–(d), respectively. The structure functions of longitudinal and transverse velocities are presented by blue solid and magenta dashed lines respectively. Inertial range for all four locations lies nearly $40 < r/\eta < 1000$. Arrows indicate that orders of structure functions increase from down to upward.

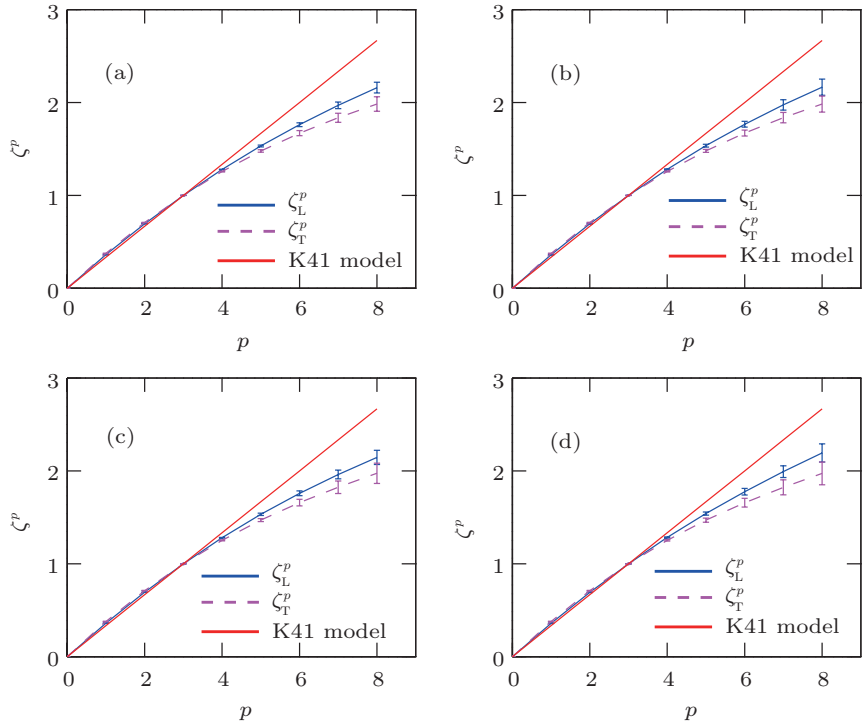


Fig. 6. (color online) Scaling exponents ζ^p/ζ^3 of longitudinal (blue solid lines) and transverse (magenta dashed lines) velocity structure functions for $p = 0,1,2,...,8$ with error bars measured at four locations, i.e., $x/M = 20,30,40$, and 48 shown in panels (a)–(d) respectively where K41 model (red solid lines) is also plotted for comparison. Error bars are defined with 95% fitting confidence.

the K41 model and ζ^p_{T} are more concaved than ζ^p_{L}, which signifies larger intermittency of transverse velocities and the differences of scaling exponents between four measured locations is small, except in the last location. It is also found from the error bars that the uncertainty of transverse scaling exponents is higher than those of longitudinal ones. To see the scaling exponents in more detail, measured values of ζ^p_{L} and the corresponding standard deviation at four locations are shown in Table 2 together with the scaling exponents calculated from two theoretical models of S–L and Zybin *et al.*[31,33]

whereas experimental and DNS measurements from Shen and Warhaft and Benzi *et al.*[6,14] are given in the last two columns. In Table 3, measured transverse scaling exponents ζ_{T}^{p} at four locations are given together with the experimental and DNS results of Shen and Warhaft and Benzi *et al.*[6,14] From Table 2, we see that our results measured at the first location are very close to the predictions of Zybin *et al.* and those measured at the last locations are close to the S–L model, experimental and recently calculated DNS scaling exponents measured at $Re_\lambda = 860$ and ≈ 600 respectively. From Table 3, the measured transverse scaling exponents, at all locations, are very close with each other with a small decreasing trend in the streamwise direction and they are within the range of known experimental and DNS results. From Fig. 6 and Tables 2 and 3, we find that the difference between longitudinal and transverse scaling exponents becomes larger with the streamwise directions, which may attribute to the decrease of Reynolds number in the streamwise direction, as shown in Table 1.

Now, let us focus on the intermittency parameter $\mu = 2 - \zeta^6$, with its most accepted longitudinal values ranging from 0.20–0.25, which is conventionally being used to quantify the intermittency corrections.[1] From Tables 2 and 3, measured longitudinal intermittency parameter μ_{L} at the first, the second, the third and the fourth locations are 0.24, 0.23, 0.24, and 0.22 respectively, whereas values of transverse intermittency parameter μ_{T}, from the first to the fourth location, are 0.33, 0.33, 0.35, and 0.34 respectively. It is clearly seen that μ_{T}s are approximately 50% larger than μ_{L}s. Our results for the transverse intermittency parameters are close to those computed by Shen and Warhaft measured from the sheared turbulence, Gotoh *et al.* and Benzi *et al.*[6,12,14] but are comparatively different from those reported by Grossman *et al.*, Bortav and Pelz, Bi and Wei, Dhruva *et al.* van de Water *et al.* and Noullez *et al.*[7,9,10,18,19,21]

Table 2. Longitudinal scaling exponents measured at four streamwise locations, i.e., at $x/M = 20, 30, 40$ and 48 by ESS. Scaling exponents calculated from two theoretical models, i.e., the She-Leveque and Zybin *et al.* models and from the work of Shen & Warhaft (2002) at $Re_\lambda \approx 860$ and Benzi *et al.* (2010) at $Re_\lambda \approx 600$, are given for comparison. Error bars are determined by averaging the number of realizations in the inertial range.

	ζ_{L}^{p} at x/M				Theory		Exp.	DNS
p	20	30	40	48	S–L	Zybin	S & W	Benzi
1	0.36±0.001	0.36±0.002	0.36±0.002	0.36±0.002	0.36	–	0.36	–
2	0.69±0.002	0.69±0.002	0.69±0.002	0.69±0.002	0.70	0.69	0.69	0.71±0.002
3	1.00	1.00	1.00	1.00	1.00	–	1.00	–
4	1.28±0.003	1.28±0.005	1.28±0.0043	1.28±0.006	1.28	1.28	1.28	1.29±0.03
5	1.53±0.010	1.54±0.015	1.54±0.012	1.54±0.0170	1.54	–	1.54	–
6	1.76±0.020	1.77±0.032	1.76±0.026	1.78±0.035	1.78	1.75	1.77	1.78±0.04
7	1.96±0.036	1.97±0.055	1.96±0.048	1.99±0.063	2.001	–	2.00	–
8	2.16±0.058	2.15±0.087	2.15±0.078	2.19±0.098	2.21	2.17	2.21	2.18±0.05

Table 3. Transverse scaling exponents measured at four streamwise locations, i.e., at $x/M = 20, 30, 40$ and 48 by ESS. Scaling exponents measured by Shen & Warhaft (2002) at $Re_\lambda \approx 860$ and Benzi *et al.* (2010) at $Re_\lambda \approx 600$, are given for comparison.

	ζ_{T}^{p} at x/M				Exp.	DNS
p	20	30	40	48	S & W	Benzi *et al.*
1	0.38±0.002	0.38±0.002	0.38±0.002	0.38±0.003	0.35	–
2	0.71±0.002	0.71±0.003	0.71±0.003	0.71±0.004	0.69	0.71±0.002
3	1.00	1.00	1.00	1.00	0.98	–
4	1.26±0.005	1.26±0.006	1.25±0.006	1.25±0.008	1.24	1.27±0.005
5	1.48±0.013	1.48±0.016	1.47±0.016	1.47±0.023	1.49	–
6	1.67±0.027	1.67±0.032	1.65±0.036	1.66±0.047	1.71	1.68±0.006
7	1.84±0.049	1.84±0.056	1.82±0.067	1.82±0.081	1.92	–
8	1.98±0.078	1.98±0.086	1.97±0.109	1.97±0.122	2.12	1.92±0.10

To further explore streamwise variation of the scaling property, let us now define an order-dependent isotropy ratio

$$I^p = \left\langle \frac{S_{\mathrm{L}}^{p}(r)}{S_{\mathrm{T}}^{p}(r)} \right\rangle, \tag{4}$$

where $\langle\cdot\rangle$ means the average within the inertial range. Note that for such a defined isotropic ratio, we have so far, for a homogeneous isotropic flow, two theoretically predicted values, i.e., $I^2 = 3/4$ and $I^4 = 9/16$ (the latter is obtained according to Eq. (3) in Section 3). The calculated ratios up to order eight at four locations are given in Table 4. Two obvious trends can ben seen from Table 4. First, the isotropic ratio decreases nearly linearly with the increases of the order num-

ber. Second, the ratio for a given order number p decreases with the increase of the distance from the grid. A more careful observation reveals that $I^2 = 0.77$ and $I^4 = 0.59$ at the last location, which are close to the exact values. The clear trend for our measured order-dependent isotropic ratios implies that the turbulent flow gradually approaches an isotropic one with the decaying of turbulence and turbulence at the last location is close to being isotropic, which may partially explain why the scaling exponent at the last location is close to the value of the She–Leveque model.

Table 4. Scale dependent mean isotropic ratios $I^p = S_{\rm L}^p/S_{\rm T}^p$ measured at four streamwise locations for scaling range $40 < r/\eta < 1000$ approximately.

p	$x/M = 20$	$x/M = 30$	$x/M = 40$	$x/M = 48$
1	0.910	0.902	0.895	0.896
2	0.814	0.800	0.787	0.767
3	0.722	0.702	0.684	0.682
4	0.636	0.614	0.591	0.586
5	0.559	0.537	0.509	0.500
6	0.490	0.471	0.439	0.423
7	0.428	0.397	0.379	0.355
8	0.373	0.368	0.327	0.296

5. Conclusion

In this article, we have measured in detail longitudinal and transverse structure functions and their scaling exponents at four different streamwise locations in a decaying, nearly isotropic turbulent flow. Streamwise evolution of structure functions, scaling exponents and order-dependent isotropic ratios at four locations have been investigated; the complicated variation of these quantities is attributed to the decrease of Reynolds number and the recovery of isotropy of turbulence with the decaying of turbulence in the streamwise direction. The main conclusions are as follows.

I. Relations between the second-order (fourth-order) longitudinal structure functions and transverse ones are reconstructed and explored. It is observed that the reconstructed transverse structure functions share the same inertial range where power-law behavior is observed, although the scaling exponents are slightly different. An important outcome of this part is that the reconstruction relation derived by Grauer *et al.* recently is less accurate as compared to the previously derived relation of Antonia *et al.*

II. Longitudinal and transverse scaling exponents are measured by ESS. No obvious trend for $\zeta_{\rm L}^p$ is observed for four streamwise locations; it is found that $\zeta_{\rm L}^P$s measured at the first location are close to the prediction of the Zybin *et al.* model, whereas the values at the last location are close to the She-Leveque model. On the other hand, transverse scaling exponents $\zeta_{\rm T}^p$ are systematically smaller than longitudinal ones of the same order as expected and they are found to become slightly smaller with the development of a streamwise direction; the transverse intermittency parameters are approximately 50% larger than the longitudinal ones at all four locations.

III. An obvious decreasing trend is found for order-dependent isotropic ratios along the streamwise direction; the turbulence at the last location is found to be close to isotropic.

Acknowledgment

We thank Prof. Meneveau for sharing his experimental data.

References

[1] Frisch U 1995 *Turbulence: The Legacy of A. N. Kolmogorov* (London: Cambridge University Press)
[2] Monin A S and Yaglom A M 1975 *Statistical Fluid Mechanics: Mechanics of Turbulence* Vol. 2 (London: Cambridge University Press)
[3] Kolmogorov A N 1962 *J. Fluid Mech.* **13** 82
[4] Moffatt H 2012 *J. Turbul.* **13** 1
[5] Biferale L and Procaccia I 2005 *Phys. Rep.* **414** 43
[6] Shen X and Warhaft Z 2002 *Phys. Fluids* **14** 370
[7] Noullez A, Wallace G, Lempert W, Miles R B and Frisch U 1997 *J. Fluid Mech.* **339** 287
[8] Camussi R, Barbagallo D, Guj G and Stella F 1996 *Phys. Fluids* **8** 1181
[9] Boratav O and Pelz R 1997 *Phys. Fluids* **9** 1400
[10] van de Water W and Herweijer J 1999 *J. Fluid Mech.* **387** 3
[11] Romano G and Antonia R 2001 *J. Fluid Mech.* **436** 231
[12] Gotoh T, Fukayama D and Nakano T 2002 *Phys. Fluids* **14** 1065
[13] Ishihara T, Gotoh T and Kaneda Y 2009 *Annu. Rev. Fluid Mech.* **41** 165
[14] Benzi R, Biferale L, Fisher R, Lamb D and Toschi F 2010 *J. Fluid Mech.* **653** 221
[15] He G, Doolen G and Chen S 1999 *Phys. Fluids* **11** 3743
[16] Hill R 2001 *J. Fluid Mech.* **434** 379
[17] Zhou T and Antonia R 2000 *J. Fluid Mech.* **406** 81
[18] Grossmann S, Lohse D and Reeh A 1997 *Phys. Fluids* **9** 3817
[19] Dhruva B, Tsuji Y and Sreenivasan K 1997 *Phys. Rev. E* **56** 4928
[20] Camussi R and Benzi R 1997 *Phys. Fluids* **9** 257
[21] Bi W and Wei Q 2003 *J. Turbul.* **4** N28
[22] Yakhot V 2001 *Phys. Rev. E* **63** 026307
[23] Kurien S and Sreenivasan K 2001 *Phys. Rev. E* **64** 056302
[24] Grauer R, Homann H and Pinton J 2012 *New J. Phys.* **14** 063016
[25] Kang H, Chester S and Meneveau C 2003 *J. Fluid Mech.* **480** 129
[26] Saddoughi S and Veeravalli S 1994 *J. Fluid Mech.* **268** 333
[27] Sreenivasan K 1996 *Phys. Fluids* **8** 189
[28] Zhou T, Pearson B and Antonia R 2001 *Fluid Dyn. Res.* **28** 127
[29] de Karman T and Howarth L 1938 *Proc. Roy. Soc. London A* **164** 192
[30] Gotoh T and Nakano T 2003 *J. Stat. Phys.* **113** 855
[31] Zybin K, Sirota V and Ilyin A 2010 *Phys. Rev. E* **82** 056324
[32] Antonia R, Ould-Rouis M, Zhu Y and Anselmet F 1997 *EuroPhys. Lett.* **37** 85
[33] She Z and Leveque L 1994 *Phys. Rev. Lett.* **72** 336
[34] Benzi R, Ciliberto S, Tripiccione R, Baudet C, Massaioli F and Succi S 1993 *Phys. Rev. E* **48** 29
[35] Benzi R, Ciliberto S, Baudet C and Chavarria G 1995 *Physica D* **80** 385